ORIGINAL RESEARCH PAPER

Anisotropy analysis in shallow marine gas hydrate bearing sediments: a case study from the offshore Mahanadi basin, India

Pradeep Kumar Shukla[1] · Dip Kumar Singha[1,2] · Kalachand Sain[3]

Abstract

Analysis of anisotropy from velocity data is essential for improving the hydrocarbon reservoir characterization. The anisotropy of a medium is affected by the mechanical strength, presence of fracture, mineral distribution of the rock, and its degree affects the seismic velocity. We attempted to characterize the anisotropy of the gas hydrate bearing sediments in the offshore Mahanadi basin using three wells. Initially, the presence of anisotropy was investigated by estimating the stiffness coefficients and Thomsen's parameters (epsilon, gamma and delta) assuming a horizontal transversely medium using dipole S-wave (upper and lower) velocities. The natural fractures were identified from the formation image data. The strong anisotropy is associated with the presence of natural fractures and lower values of the elastic modulus. Most of the strong and weak anisotropy zones are oriented in the NW to W direction of the study area. Our study suggests that the anisotropy in gas hydrate bearing sediment is stress-induced due to the presence of pore filling fractures, and the change of mechanical behavior. The higher positive values of epsilon and delta with gamma represent either dry solid gas hydrate or free gas filled in the fracture of the sediments as observed in the crossplot analysis. Finally, we modeled P-wave and S-wave velocities by incorporating the Thomsen's parameters. S-wave velocity is less effective than P-wave velocity at 90° angle of fracture relative to the symmetry axis and the modeled P-wave velocity increases upto 2.8% in the gas hydrate bearing sediments.

Keywords Anisotropy · Thomsen's parameter · DSI dipole shear wave · Natural fractures · Elastic parameters · Gas hydrate · Offshore Mahanadi basin

Introduction

Gas hydrates are ice-like crystalline solid substances that are composed mainly of methane and water in low temperature and high-pressure environments (Lee and Collett 2012). It occurs in shallow marine sediments of the outer continental margin of the deep offshore basin. The markers of gas hydrate are anomalous seismic bottom simulating reflectors (BSR), gas chimney, and seismic amplitude attenuation or blanking observed in high resolution multi-channel seismic (MCS) data (Sain and

Gupta 2008, 2012; Coffin et al. 2007). Gas hydrate sediments show relatively higher seismic velocity than sediments without gas hydrates. These have been identified in multi-channel seismic (MCS) data in the deep offshore Mahanadi basin (Singha et al. 2019; Sain et al. 2012). As gas hydrates occur mainly in fracture filings, veins, and pore filling of the shallow marine sediments in the study area of the Mahanadi basin, the physical properties of gas hydrate sediments change and produce anisotropy consequently (Kumar et al. 2014; Shankar and Riedel 2014). The assessment of a gas hydrate reservoir is done by computing petro-physical parameters such as saturation, porosity and permeability using geophysical well log data (especially P- and S-wave velocity) which are also affected by the several geological factors, anisotropic property and its degree (Shankar and Ridel 2014; Lee and Collett 2012). The anisotropy affects the amplitude of MCS in the azimuth in the transverse component (Satyavani et al. 2013). Anisotropy caused by fractured gas hydrate in Krishna-Godavari and Mahanadi basin was previously reported by

✉ Dip Kumar Singha
dipgeo89@gmail.com; dipkrsingha@bhu.ac.in

[1] Department of Geophysics, Institute of Science, BHU, Varanasi 221005, India

[2] Department of Geology and Geophysics, IIT Kharagpur, Kharagpur 721032, India

[3] Wadia Institute of Himalayan Geology, Dehradun 248001, India

Gosh et al. (2010), Kumar et al. (2006), Lee and Collett (2012), Cook et al. (2010) and Shankar and Pandey (2019). Therefore, for accurate assessment and characterization of gas hydrates from seismic velocity and other rock properties, a study of anisotropy from well log data must be required in the gas hydrate bearing sediments of the Mahanadi basin. The anisotropy of rock means variation of a physical property with direction or rock property is direction dependent (Tatham et al 1991; Sill et al. 2012). In sedimentary rocks, two types of anisotropy are prevalent: one is intrinsic type anisotropy defined as platy nature of thin isotropic layers such as shale/clay and another is associated with stress induced anisotropy due to the formation of elongated voids, shape of the particles, voids, and natural fracture alignments (Jaeger and Cook 1979; Prioul et al. 2007; Bidgoli and Jing 2014). The anisotropy due to layering is modeled as vertical transverse isotropy (VTI) whereas stress-induced anisotropy is generally modeled as horizontal transverse isotropy (HTI) in most cases (Wang 2002; Sill et al. 2012). Here we do not consider VTI because it requires a thick overburden and thin shale layering which is not found in the depth of interest below the seafloor in the study area. The presence of vertical fractures/joints and preferred alignments by grain or pore filling is common and thus, it makes sense to assume an HTI medium for a description of sediments in our analysis (Sayers 1994, 2005; Wang 2002; Sill et al. 2013). Moreover, these sediments might be VTI, but the presence of fractures makes HTI a much better description of the sediments since the fractures, not the bedding, control the anisotropy. The sediment's thickness varies 180–200 m above BSR which mainly contains highly unconsolidated gas hydrate sediments with clay/silt marine sediments. The gas hydrate is present in clay/silt-based fracture medium in the eastern offshore basin of India (Lee and Collett 2012; Sain et al. 2012; Kumar et al. 2014).

For a vertical well, the parameters of an anisotropy medium are defined by the Thomsen's parameters for a VTI medium (Thomsen 1986, 1999; Sill et al. 2012; Sill 2013). Thomsen's parameters and fracture density have been calculated for wells at National Gas Hydrates Program (NGHP)-expedition-01 drilling sites of the offshore Mahanadi basin for understanding their effects on rock property.

The objectives of this study are to compute the (a) stiffness coefficients and Thomsen's parameters (epsilon, gamma and delta) for HTI medium at NGHP-01-19, (b) anisotropy coefficient and fracture density from P-wave velocity and dipole shear data, (c) natural fracture and orientation from formation micro image log (FMI), (d) synthetic model of S-wave estimation, (e) estimation of elastic parameters in isotropic and anisotropic medium and (f) modeling of P-wave and S-wave using Thomsen's parameters.

Geological setting of study area

The Mahanadi basin is a significant hydrocarbon basin located in the northern side of eastern passive continental margin (ECMI). The offshore basin is in the Bay of Bengal surrounded by the Bengal basin in north east and Krishna-Godavari basin in south-west covering an area of 14,000 sq. km in the sea (Bastia and Nayak 2006; Bastia et al. 2014) as seen in Fig. 1. The margin evolved during Permo-Trassic geologic time due to rifting and break-up of the Gondwana supercontinent (Sastri et al. 1981; Sastri et al. 1973).

The major faults are lying with a dominant orientation ENE-WSW: NNE–SSW and NNW–SSE are parallel/sub-parallel to the present-day coastline of the basin (Das et al. 2010; Fuloria et al. 1992) (Fig. 2). The rift structure of Jurassic age along the eastern continental margin is cutting across older NW–SE-trending in Permian–Triassic age (Sastri et al. 1981; Ramana et al. 1981). Two rivers mainly Mahanadi and Godavari discharge the sediments upto the continental margin in the offshore basin (Sastri et al. 1981; Biksham and Subrahmanyam 1988) and the sediments become thicker reaching up to about 8 km because of the collision of Indian plate with Eurasia in early Miocene age. The geologic age of the sediment in the deep offshore is from upper Cretaceous to recent age (Jagannathan et al. 1983; Fuloria et al. 1992; Fuloria 1993). Many geological features such as the regional fans, cut-and-fill channels and abundant growth faults are observed in offshore due to the deposition of sediments (Bastia et al. 2014; Bastia and Nayak 2006). The deep-water deposits are identified by interpreted high resolution seismic data which indicates the presence of potential hydrocarbon reservoirs in the offshore Mahanadi basin (Bastia and Nayak 2006; Kumar et al. 2014). High sediment rate (20–40 cm/kyr), high total organic matter and geothermal gradients of 35–45 °C/km may show indication of gas hydrate reservoir in the deep offshore where low temperature and high pressure satisfy the favorable condition in the basin (Singha et al. 2019, Sain et al. 2011; Shankar et al. 2013; Kumar et al. 2014 and Collette et al. 2008). The gas hydrate is deposited with clay/silt sediments and fracture zones of Pleistocene age in the deep water in the basin. The evidence of gas hydrates are identified by logging while drilling (LWD) and temperature of core sample by IR camera at NGHP-01 sites in the offshore Mahanadi basin (Kumar et al. 2014; Rai et al. 2020; Sain and Gupta 2012).

Fig. 1 **a** National gas hydrate program expectation 01 (NGHP-01) drill site map depicting the modified location of the drill sites established during the expectation in the Mahanadi basin (after Kumar et al. 2014). **b** Modified Bathymetric map depicting the location of the research drill sites established in the Mahanadi basin (after Kumar et al. 2014; Singha et al. 2019)
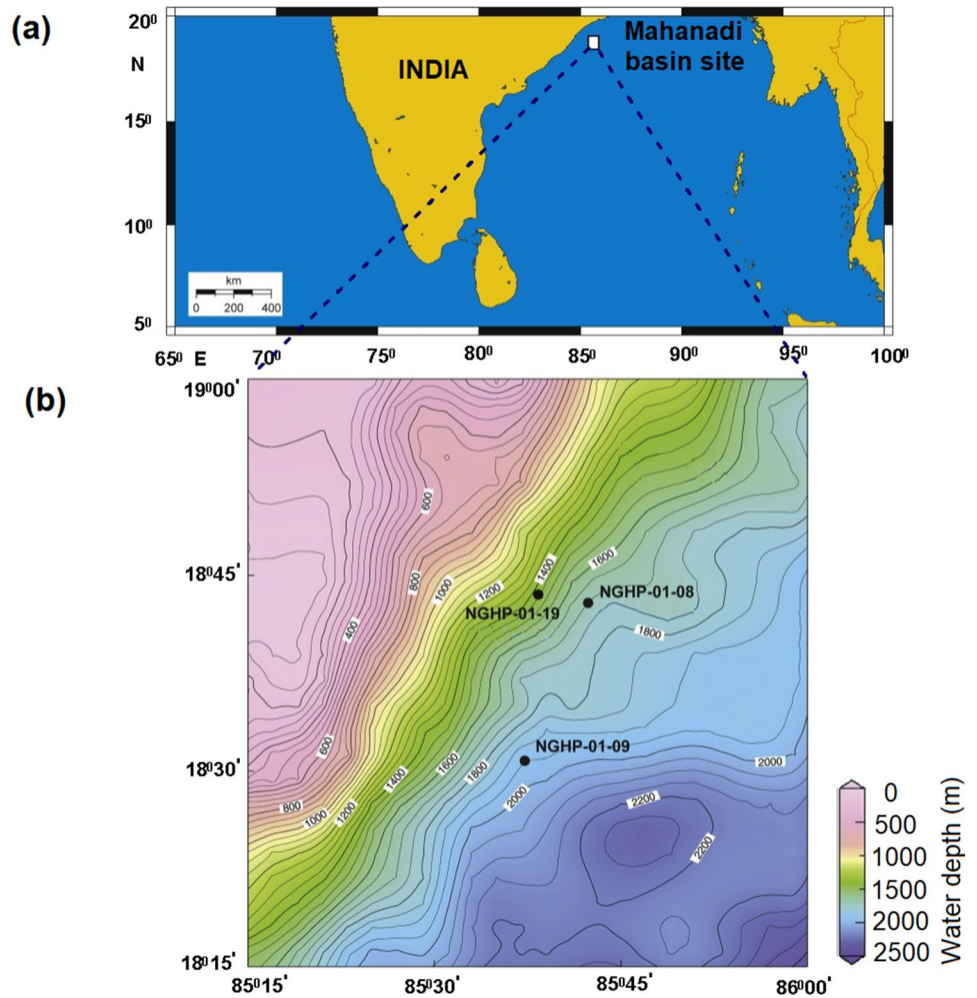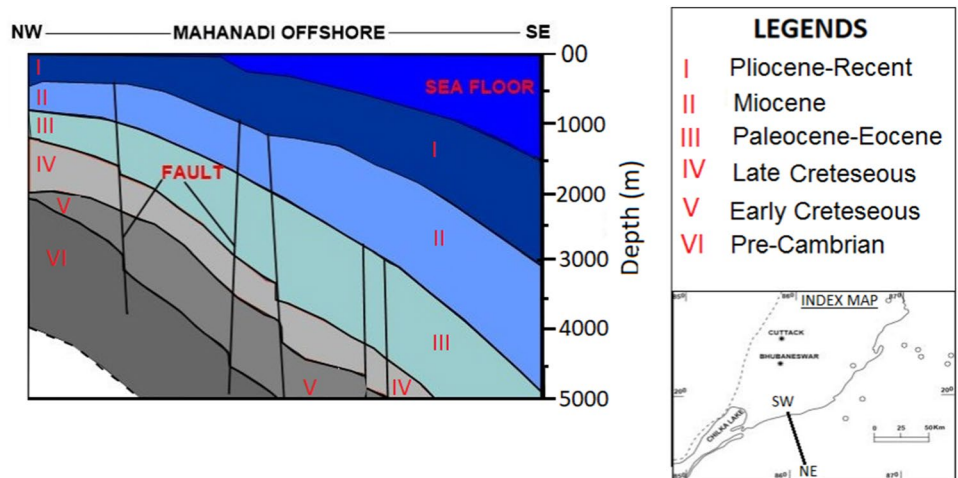

Fig. 2 Geological cross section in the Mahanadi offshore basin, India near the study area at NGHP-01 sites (after Fuloria et al. 1992)
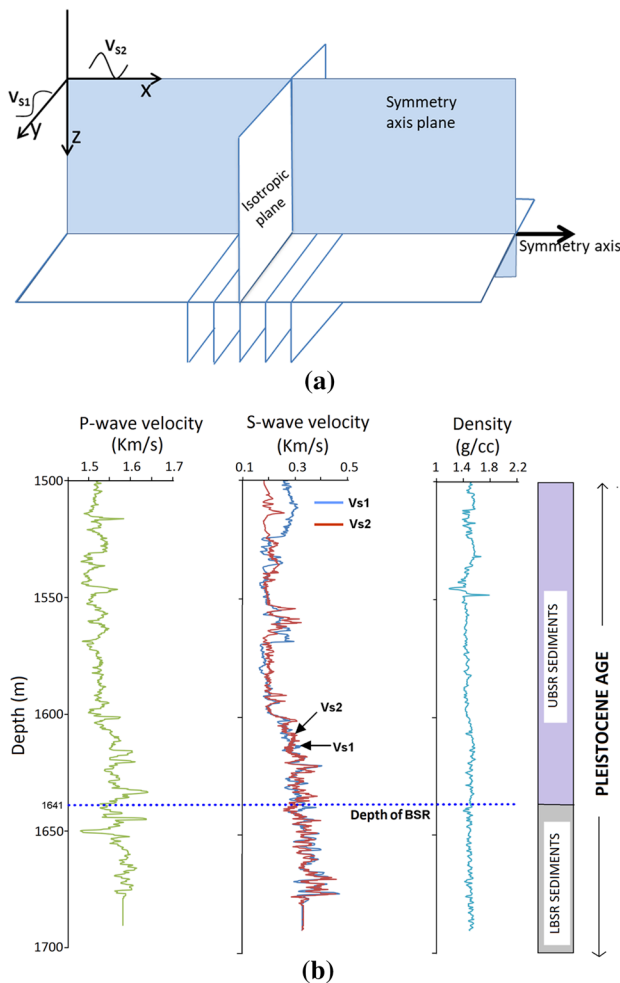
Fig. 3 a Graphical presentation of symmetric axis and isotropic plane for an horizontal transverse medium (HTI) where upper dipole shear mode wave (V_{S1}) and lower dipole shear mode wave (V_{S2}) which are along with axis of symmetry (isotropic plane) and perpendicular to the axis of symmetry respectively. **b** P-wave velocity, V_{S1}, V_{S2} and density varying with depth in gas hydrates bearing sediments and depth of BSR is 1641 m at NGHP-01-19 site

Material and method

With the presence of fractures and faults in marine gas hydrate-bearing sediments of the offshore basin (Singha et al. 2019; Collett et al. 2008), we have assumed azimuthal anisotropy for characterization of the hydrate reservoir. The most common approach for modeling stress-induced or azimuthal anisotropy is to consider angular of penny shape fractures for a vertical well (Gupta 1973, Sill et al. 2010, 2012; Sill 2012). The azimuthal anisotropy here is represented by transverse isotropy with a horizontal axis of symmetry (HTI) as shown in Fig. 3a. In the figure, the symmetry axis of HTI is along the direction of the x-axis and the plane (x, z) containing the symmetry

axis is referred to as the symmetry axis plane. For a vertical well, S- wave is polarized in two components; one is propagating along symmetric plane while the other propagates along fracture isotropic (Sill 2012; Satyavani et al. 2013). Here, we have used the upper shear mode (V_{S1}) and lower shear mode (V_{S2}) wave of S-dipole data measured by the dipolar sonic tool (DSI) at NGHP-01-19 as shown in Fig. 3b. V_{S1} mode is considered to propagate along isotropic plane whereas V_{S2} mode is traveling along the symmetry axis. Dipole shear data were not recorded in the remaining wells at NGHP-01-09 and NGHP-01-08, but all conventional data such as P-wave velocity, density, gamma, resistivity, neutron porosity and formation image log (FMI) are available for these wells. The wells (NGHP-01-19, NGHP-01-09 and NGHP-01-08) are located at a water depth of 1433 m, 1935 m, and 1701 m, and the total drilled depth area 280mbsf, 330mbsf, and 350mbsf for above mentioned wells respectively. Based on log data analysis, the BSR of the three wells is observed at depths of 208 m, 290 m, and 257 m respectively below seafloor (mbsf) at this site of the Mahanadi offshore. Quality of V_{S1} and V_{S2} is poor up to a depth of 90 mbsf but the coherence of waveform of upper and lower are of good quality above and below the BSR (~ 1641 m) shown in upper and lower BSR (UBSR and LBSR) in Fig. 3b.

The effect of gas hydrates sediments in anisotropy medium (HTI) is investigated by Thomson's coefficients. Thomsen (1986) first introduced three dimensionless anisotropic parameters. The coefficient, epsilon is related to P-wave anisotropy and gamma relates to S-wave anisotropy while delta is a critical factor that depends on the shape of P- and S-wave surfaces. P-wave anisotropy is the fractional differences between vertical P-wave i.e. V_P (90°) velocity and horizontal P-wave velocity i.e. V_P (0°) which is earlier defined as epsilon (ε) (Wang 2002) and similarly S-wave velocity is the fractional difference between SV and SH velocity which is earlier defined as gamma (γ). These parameters are computed from stiffness coefficients which are used for a fractured medium with given fracture density in HTI medium (Hudson 1980).

Determination of stiffness coefficients

In this regard, applying General Hooke's law for the non-vanishing elastic stiffness coefficients C_{ij} (Ostadhassan et al. 2012) for an HTI medium with respect to the symmetry axis, the stiffness tensor has five independent components which are related with each other. The symmetric six by six matrices with elastic stiffness coefficients for HTI are represented as below (Musgrave 1970).

Fig. 4 Stiffness coefficients such as C_{11}, C_{33}, C_{44}, C_{66} and C_{13} respectively using P-wave, V_{S1} and V_{S2} from DSI tool for an horizontal transverse medium (HTI) in the well NGHP-01-19

In HTI medium, some of stiffness coefficients are equal to each other as follows;
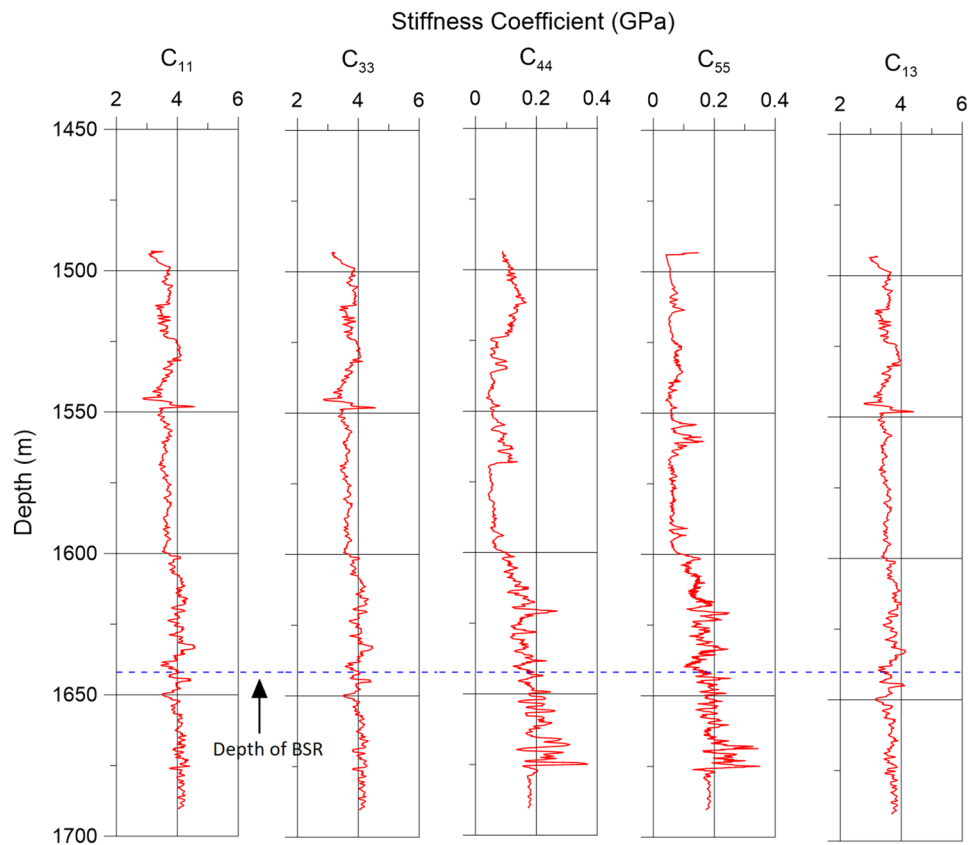
$$C_{ij} = \begin{bmatrix} C_{11} & C_{13} & C_{13} & 0 & 0 & 0 \\ C_{13} & C_{33} & (C_{33} - 2C_{44}) & 0 & 0 & 0 \\ C_{13} & (C_{33} - 2C_{44}) & C_{33} & 0 & 0 & 0 \\ 0 & 0 & 0 & C_{44} & 0 & 0 \\ 0 & 0 & 0 & 0 & C_{55} & 0 \\ 0 & 0 & 0 & 0 & 0 & C_{55} \end{bmatrix} \quad (1)$$

$C_{22} = C_{33}$, $C_{55} = C_{66}$, $C_{32} = C_{23} = C_{33} - 2C_{44}$, $C_{13} = C_{12}$,

The polarized S-wave velocities in an HTI medium can be written as (Wang 2002):

$$\rho V^2_{S1} = C_{44}, \quad (2)$$

and

$$\rho V^2_{S2} = C_{55}, \quad (3)$$

As vertical the well at NGHP-01-19 site was drilled perpendicular to the sedimentary bedding plane, only three of these five independent moduli using the stiffness coefficients (C_{33}, C_{44}, and C_{66}) can be measured by dipole shear data.

$$C_{33} = \rho V^2_P = \lambda + 2\mu, \quad (4)$$

where, λ is Lame's constant and μ is shear modulus or rigidity.

Also, in HTI medium (Sil 2012)

$$C_{55} = C_{66} = \rho V^2_{S2}, \quad (5)$$

As no core data is available, other stiffness coefficients (C_{11} and C_{13}) can be estimated from Annie model proposed by (Schoenberg and Sayers 1995). The constants C_{13} and C_{11} are given below,

$$C_{11} - C_{33} = 2(C_{66} - C_{44}) \quad (6)$$

and

$$C_{13} + 2C_{44} - C_{33} = 0 \quad (7)$$

Using Eqs. (6) and (7), we can estimate all five independent stiffness coefficients. Further, Thomsen's parameters such as gamma, epsilon and delta for an HTI medium can be estimated using these coefficients. The shear modulus is related to coefficient given below.

$$C_{44} = \rho V^2_{S1} = \mu, \quad (8)$$

Estimated stiffness coefficients such as C_{11}, C_{13}, C_{33}, C_{44} and C_{55} are the five independent stiffness moduli in HTI medium show lower values in the gas hydrate sediments

Table 1 Stiffness coefficient such as C_{11}, C_{13}, C_{33}, C_{44} and C_{66} using upper and lower dipole shear velocities and P-wave data in above and below BSR

	C_{11}(GPa)			C_{13} (GPa)			C_{33} (GPa)			C_{44} (GPa)			$C_{55} = C_{66}$ (GPa)		
	Min	Max	Avg	Min	Max	Avg	Min	Max	Avg	Min	Max	Avg	Min	Max	Avg
UBSR	2.86	4.575	3.738	2.954	3.972	3.534	2.849	4.560	3.754	0.036	0.268	0.0984	0.0409	0.249	0.090
LBSR	3.460	4.44	4.025	2.776	4.400	3.593	3.505	4.419	4.035	0.123	0.368	0.197	0.100	0.348	0.191

and the values increase below BSR where free gas is present (Fig. 4). The minimum, maximum and average values of stiffness coefficients are listed in (Table 1) for upper BSR (UBSR) of the depth interval 1550 to 1641 m and lower BSR (LBSR) of depth interval 1641 to 1690 in the well NGHP-01-19.

Estimation of Thomsen's parameter

Using the following, we have estimated Thomsen's parameters ε, γ and δ given below (Rüger 1998a, b):

$$\varepsilon = \frac{C_{11} - C_{33}}{2C_{33}}, \qquad (9)$$

$$\gamma = \frac{(C_{55} - C_{44})}{2C_{44}}, \qquad (10)$$

and

$$\delta = \frac{(C_{13} + C_{55})^2 - (C_{33} - C_{55})^2}{2C_{33}(C_{33} - C_{55})}, \qquad (11)$$

We notice a relation among these Thomsen's parameters—first when ε remains constant, δ increases with decrease of γ; when γ is constant, δ will increase with ε; lastly when ε is approximately equal to γ, and then δ generally increases with degree of anisotropy (Ostadhassan et al. 2012; Mavko et al. 1995).

Determination of fracture density

We can write γ in terms of tangential fracture compliance, Z_T (Liu et al. 2000) as,

$$\gamma = \frac{-1}{2}\mu Z_T, \qquad (12)$$

For the tangential Z_T, it is given by (Sayers and Kachanov 1995),

$$\frac{Z_N}{Z_T} = 1 - \frac{\sigma}{2}, \qquad (13)$$

where, Z_N is the normal fracture compliance and σ is the Poisson's ratio of the medium. The Poisson's (σ) ratio can be derived using the V_P/V_{S1} ratio (Mohammed and Zillur 2001; Potter and Foltinek 1997);

$$\sigma = \frac{1}{2}\frac{\left((V_p/V_{s1})^2 - 2\right)}{\left((V_p/V_{s1})^2 - 1\right)}, \qquad (14)$$

The significance of the ratio of Z_N/Z_T is that high values greater than 0.8 indicate the presence of gas-filled fractures and values less than 0.5 represent water-filled fractures (Sill 2012). In our study area, the free gas is assumed to be present below the BSR in the un-compacted fracture clay/silt with Poisson's ratio varying from 0.38 to 0.40. Therefore, our computed Z_N/Z_T using Eq. (13) is approximately 0.8 that indicates gas-filled fractures. Also, we can easily compute the normal fracture weakness parameter; δ_N (Schoenberg and Sayers 1995) from the values of Z_N/Z_T, and background P-wave, S-wave and density.

$$\delta_N = \frac{Z_N M_b}{1 + Z_N M_b}, \qquad (15)$$

where, $M_b = \lambda + 2\mu = C_{33}$

Further, the fracture density can be calculated using the following equation (Sill 2012; Shaw and Sen 2006):

$$e = \frac{3\delta_N(3 - 2g)}{16}, \qquad (16)$$

where, e is the fracture density; g is the ratio of square of vertical V_P and V_S wave velocity. A negative value of fracture density shows weak anisotropy zone and positive shows strong anisotropy zone.

By following all the steps and equations described above, we have computed the anisotropic parameters such as ε, γ and δ reaching maximum value below the depth of 1550 m indicating the presence of strong anisotropy in the well NGHP-01-19 (Fig. 5). A high value of fracture density at several depth intervals marked by red circles seen in Fig. 5 is clear indication of presence of anisotropy in the uncompacted gas hydrate bearing sediments. We consider this as stress induced anisotropy because we have found many fractures and breakouts in the unconsolidated shallow marine sediments in the image log data at NGHP-01 site and the

Fig. 5 Computed Thomsen's parameters for the analysis of anisotropy such as gamma ray log value in API, fracture density, epsilon, gamma and, delta for horizontal transverse medium (HTI) from upper and lower BSR. Higher fracture densities values are marked by red circle are for corresponding to the higher values of Thomson's parameters such as epsilon, gamma and delta
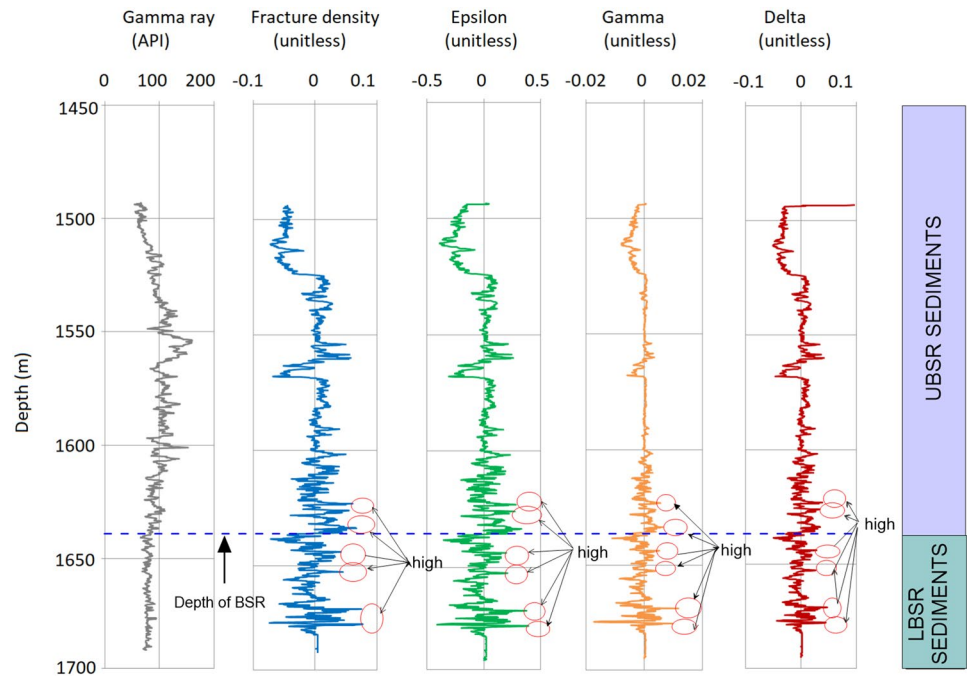

Table 2 Thomsen's parameters such as epsilon (ε), gamma (γ) and delta (δ) computed from stiffness coefficient for an HTI medium for the well NGHP-01-19 in above and below BSR

	Epsilon (ε) Dimensionless unit			Gamma (γ) Dimensionless unit			Delta (δ) Dimensionless unit		
	Min	Max	Avg	Min	Max	Avg	Min	Max	Avg
UBSR	− 0.0259	0.0203	− 0.0022	− 0.0027	0.0023	− 0.00026	− 0.0518	0.040	− 0.0044
LBSR	− 0.0253	0.022	− 0.0013	− 0.0061	0.0043	− 0.00029	− 0.0506	0.0456	− 0.002

gas hydrates mainly deposited in fracture pore filled in clay/silt dominated fine grain sediments, those will be discussed in the Sect. 4. The stress induced anisotropy is caused by uneven stress in the sedimentary rock that is responsible for azimuthal variation of stress concentration around the borehole (Fang et al. 2013; Sayer 2002; Ruger 1998a, b). As a consequence the share wave velocity varies azimuthally around the borehole (Ruger 1998a; b). The minimum, maximum and average values of ε, γ and δ for the well NGHP-01-19 are listed in Table 2.

Estimation of anisotropy coefficient from S-wave

Anisotropy coefficient from S-wave data is another important parameter for measuring the degree of anisotropy, i.e., whether it is strong or weak. It can be estimated using the velocity relationship of shear-wave velocities (V_{S1} and V_{S2}) from the well log data. The anisotropy coefficient (A_b) is determined by the following equations (Yan 2002)

$$A_b = \frac{Vs1 - Vs2}{\acute{V}s}, \qquad (17)$$

where,

$$\acute{V}s = \frac{Vs1 + Vs2}{2},$$

Our data shows that the anisotropy coefficients value increases and the maximum value of anisotropy are about 0.47 in the depth range of 1551 m to 1575 m, thus this is a strong anisotropy zone (Fig. 6). As the values of V_{S1} are not always higher than the values of V_{S2} throughout the depth in the well, the anisotropy coefficient from S-wave velocity we are getting sometimes negative values. The intermediate anisotropic zone may have the values in range -0.2 to 0.3. It is also noticed that the values of anisotropy coefficients are high for higher values of fracture density and Thomson's parameters in free gas zone is higher than that in the gas hydrate zone in the well NGHP-01-19.

Natural fractures observed in FMI log

Natural fractures are joints or discontinuity in the surface, which are expressed by cracks, fissures, or faults in the rock (Twiss and Moores 1992; Zoback et al. 1985). Solid gas hydrates fill most of the natural fracture, converting an open

Fig. 6 Computed anisotropy coefficient using V_{S1}, V_{S2} and P-wave and maximum value is ~ 0.47 in the strong anisotropy zone of depth interval 1600 to 1645 m as marked by green circle
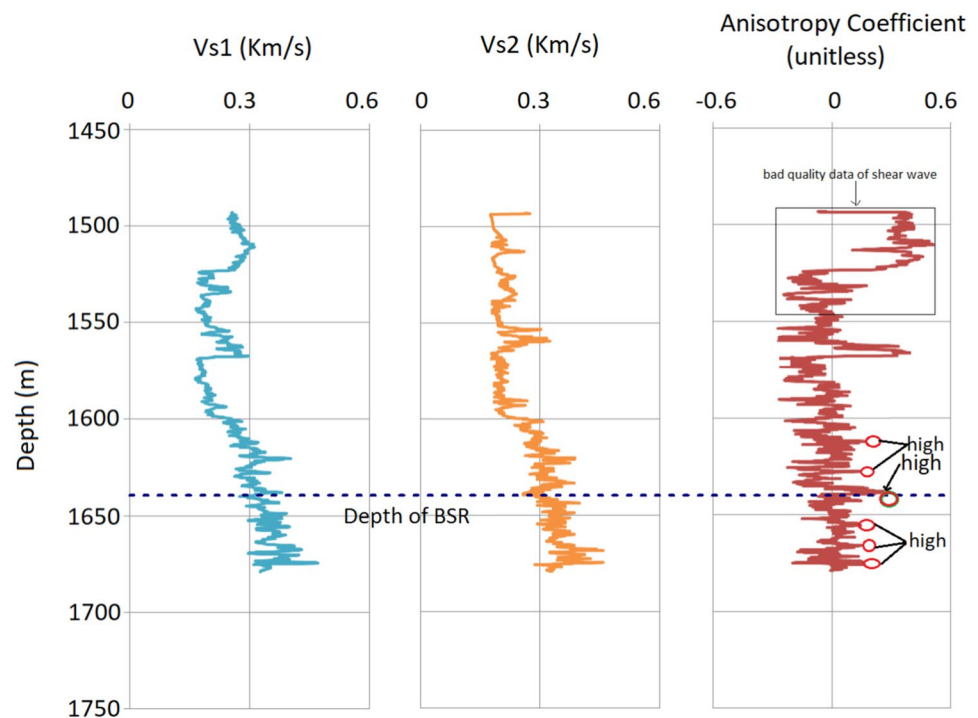
fracture to a sealed fracture. The natural fractures are subdivided into the open fracture, partially open fracture and resistive fracture (Rajabi et al. 2010; Esmersoy et al. 1995). The presence of the natural fractures influences the stress-induced anisotropy in the gas hydrate sediments.

These fractures appear in the formation micro image (FMI) log as a sinusoidal or half sinusoidal as the projection of a planar intersection with a cylindrical borehole. The FMI is a resistivity imaging tool consisting of two perpendicular pairs of caliper arms, with the end of each arm hosting a pad and attached flap. The pads and flaps contain typically 24 resistivity sensors on each pad or flap. The resistivity data from this log can be processed to build up a picture of the wellbore wall based on resistivity contrasts (Ekstrom et al. 1987; Rajabi et al. 2010; Chatterjee and Singha 2018). The dip and azimuth of the fractures for a vertical well can be calculated from a sinusoidal appearance by the following formula:

$$\theta = \tan^{-1} h/d, \tag{18}$$

where, h = length from crest to trough, d = diameter of borehole and θ = dip angle of fracture.

b. Examples of resistive fracture and dip for NGHP-01-19, NGHP-01-09 and NGHP-01-08 are shown in Fig. 7. The orientations of strong and weak anisotropy are N320° and N351.5° for well NGHP-01-19 respectively as shown in Fig. 8a, b. The well NGHP-01-09 located towards the south holds total 38 fracture sets with dip amount ranging from 10.45° to 38.15° as shown in Fig. 7c, d and orientation N198.6° in strong anisotropy and N136.6° in weak zone as shown in Fig. 8c, d. The least number of fractures are present in well NGHP-01-08 located eastward with dip amount 21.0° shown in Fig. 7e, f and orientation N344.6° in strong anisotropy and N345.7° in weak zone shown in Fig. 8e, f. The number of fractures with dip amount and orientation for three wells are listed in Table 3.

Estimation of S-wave velocity

Only the NGHP-01-19 contains S-wave data and synthetic S-wave data are estimated for the remaining wells NGHP-01-09 and NGHP-01-08 respectively. To do so, we first use Castagna's equation between P-wave veloc-

$$\text{Azimuth of fracture } = \text{ dip direction} + 90°(\text{dip azimuth is calculated from the position of the Trough}) \tag{19}$$

The well NGHP-01-19 contains 25 fractures observed from the FMI log in several depth intervals. The dip and orientation of the fractures vary from 11.3° to 36.91° and N166.15° to N360° respectively as demonstrated in Fig. 7a,

ity and S-wave velocity for gas hydrate sediments of the study area with coefficients that match the predicted shear velocity. The estimated S-wave velocity is matched separately with V_{S1} and V_{S2} with changing the coefficients
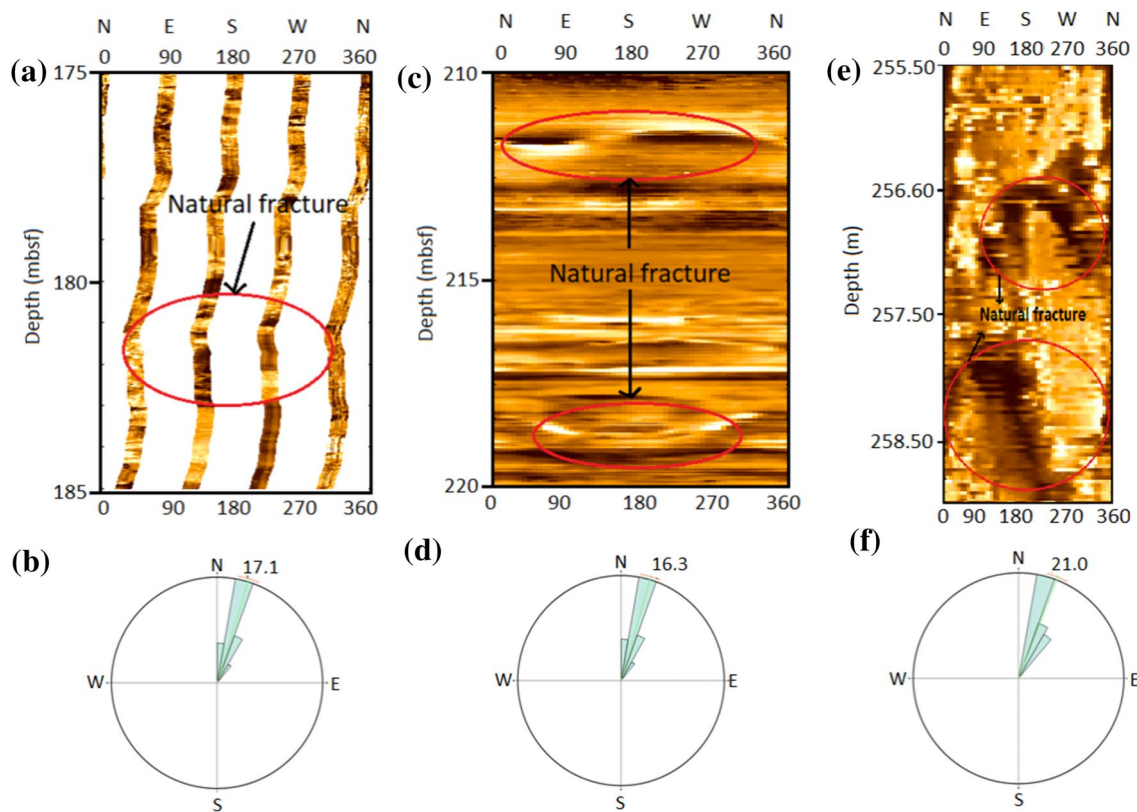
Fig. 7 Natural fractures marked by red circle and corresponding the rose diagram for the orientation of the total natural fractures, **a** and **b** for well NGHP-01-19, **c** and **d** for NGHP-01-09 and **e** and **f** for well NGHP-01-08 respectively

('a' and 'b'). As, the shear wave velocity was affected by the unconsolidated sediments below the seafloor, based on this statistical approach, we performed the better correlation between the predicted shear wave velocity and the dipole sonic velocity. We obtained for coefficients values 1.452 and 1.031 between estimated S-wave and V_{S1} with goodness of fit (R^2) ~ 0.70 (Fig. 9a). The poorer match was observed between estimated S-wave and V_{S2} with R^2 ~ 0.51 in Fig. 9b. Therefore, V_{S1} was chosen to establish the equation with P-wave velocity and we have used V_{S1} for computation of elastic parameters in other wells where no availability of S-wave velocity. Thus we obtained the following modified empirical relationship for gas hydrate-bearing sediments in the Mahanadi offshore;

$$V_P = 1.452V_S + 1.031 \tag{20}$$

where, V_P and V_S refer to P-wave and S-wave velocities in km/s respectively.

Using this modified empirical relation, we estimate the S-wave velocity at other well sites where no recorded S-wave data is available.

Computation of elastic parameters

Elastic properties in an isotropic elastic medium are affected by stress causing anisotropy (Ruger 2002). Stress-induced anisotropy does influence the elastic properties under the state of hydrostatic pressure. In other way, stress-induced anisotropy can be applied for the spatially varying anisotropic elastic constants that are required for the forward modeling of wave propagation in a borehole under a given pressure condition, i.e. hydrostatic pressure (Fang et al. 2013). In the study area, the observed stress is normal followed by the hydrostatic pressure (Singha et al. 2019) whereas the velocity and density are not enough high to influence the elastic properties as unconsolidated sediments contains mostly muds (Winkler 1996). We examine various elastic parameters such as young's modulus, bulk modulus, shear modulus, and Poisson's ratio in both media i.e. isotropic and anisotropic. The rock elastic parameters are seen to have sharp changes in Thomsen's parameters as well as fracture density in the strong and weak anisotropy zones.
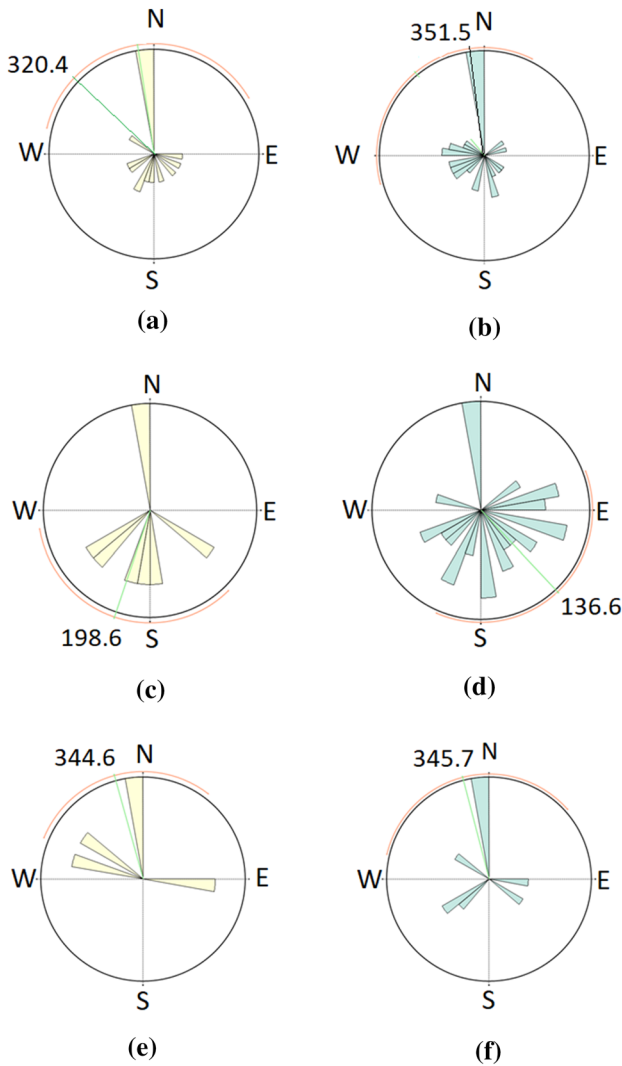
Fig. 8 Orientation of strong and weak anisotropy based on the orientation of natural fractures, **a** and **b** for well NGHP-01-19, **c** and **d** for NGHP-01-09 and **e** and **f** for well NGHP-01-08 respectively

Isotropic medium

The elastic moduli have been estimated from V_P, V_S and density (ρ) log data using the equations provided by (Potter and Foltinek 1997).

Shear modulus, $\mu = V_s^2 \rho$ (21)

Young's modulus $Y = 2 * \mu (1 + \sigma)$ (22)

Bulk modulus, $K = \rho * \left(V_P^2 - \frac{4}{3} V_S^2 \right)$ (23)

Anisotropic medium

The elastic moduli have been computed from P- wave and S-wave relates stiffness coefficient for HTI medium such as C_{33}, C_{44}, and C_{55} by Wang 2002.

Shear modulus, $\mu = C_{44}$ (24)

Young's modulus, $Y = 2 * C_{44} * (1 + \sigma)$, (25)

Bulk modulus, $K = C_{33} - C_{55} * (4/3)$ (26)

The elastic parameters were calculated from log data for NGHP-01-19 in both the mediums while from synthetic shear data for NGHP-01-09 and NGHP-01-08 in only isotropic medium because of unavailability of S-wave velocity (Figs. 10, 11 and 12). To fully describe TI, we need both vertical and horizontal section of well which will improve anisotropy estimation. As we are using only vertical velocity, therefore, elastic properties obtained from these logs are isotropic in nature. No such significant differences are observed in the values of the elastic parameters for the isotropic and anisotropic medium at NGHP-01 wells shown in Fig. 10. But, the elastic parameters are seen to be increasing from UBSR to LBSR while the Poisson's ratio decreases. Elastic properties of gas hydrate-bearing sediments are similar to those of the unconsolidated sediments. From the above analysis, it is clear that if the normal fracture weakness increases then fracture density also increases. Therefore, the rock elastic coefficient values decrease at that depth zone because rock elastic moduli values are directly proportional to the stiffness coefficient values. The values of the stiffness coefficients are inversely proportional to the fracture density values. The low range of elastic modulus values gives a high range of fracture density values showing a strong range/zone of anisotropy and vice versa as clearly noticed in Fig. 10 marked by the red circles.

Table 3 Natural fractures for three wells with dip amount and dip orientation at NGHP-01 sites

Wells	Natural fracture	Orientation (°)			Dip amount (°)			Dip SD*
		Min	Max	Average	Min	Max	Average	
NGHP-01-19	25	N166.15	N360	N332.8	11.3	36.91	16.3	±4.75
NGHP-01-09	38	N51.42	N360	N164.2	10.45	38.15	17.14	±5.89
NGHP-01-08	20	N92.57	N360	N328.4	10.52	32.73	21.0	±5.88

Fig. 9 **a** A synthetic model between P-wave and S-wave (V_{S1}) in km/s with goodness of fit R^2 is 0.612. **b** A statistical linear relationship established between S-wave (V_{S1}) and estimated S-wave from modified Castagna's empirical relation in with goodness of fit R^2 is 0.701
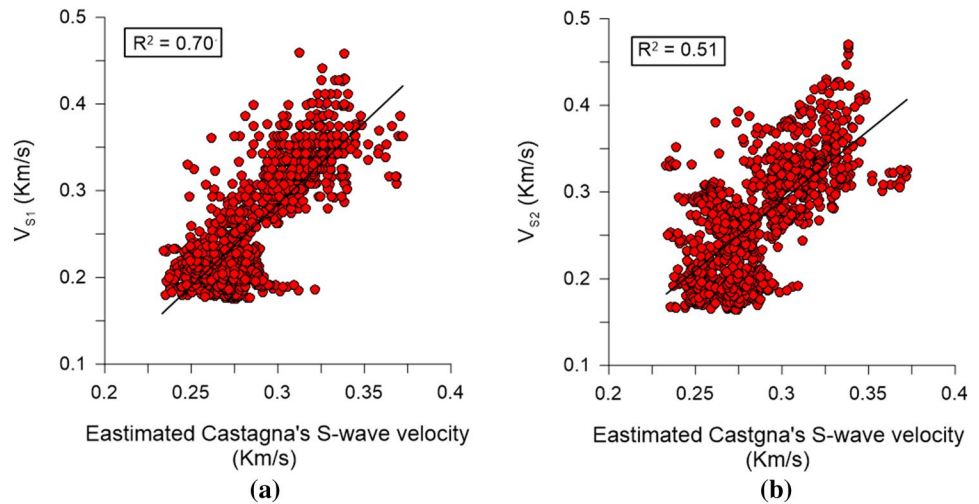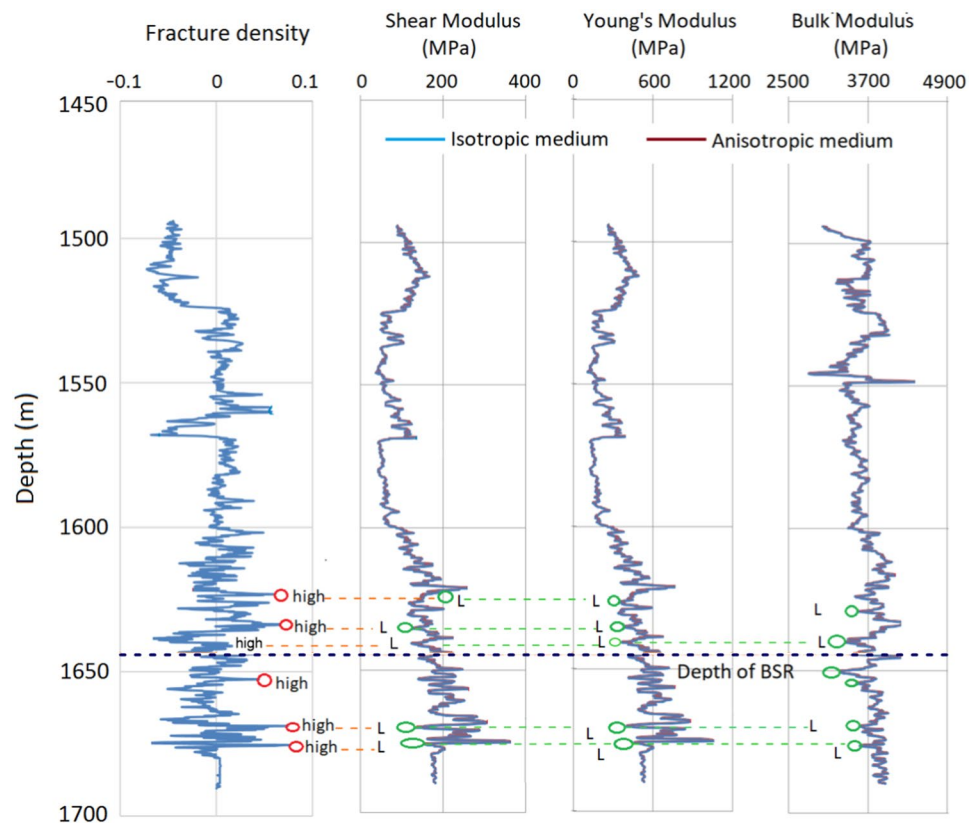

Fig. 10 Changes of elastic parameter such as shear modulus, young's modulus and bulk modulus with fracture density at the depth of anisotropy in the well NGHP-01-19. The lower elastic values (denoted by L) are found across the higher fracture density values indicating strong anisotropy


Results

For a horizontal transversely isotropic medium the stiffness coefficient C_{11}, C_{13}, C_{33}, C_{44} and C_{55} are increasing from depth interval 1400 to 1690.32 m for the well NGHP-01-19. The average values of the stiffness coefficients are 3.738 GPa, 3.534 GPa, 3.754 GPa, 0.0984 GPa and 0.090 GPa respectively in the sediments above the BSR.

The average stiffness values are slightly increased below the BSR which are 4.025 GPa, 3.593 GPa, 4.035 GPa, 0.197 GPa and 0.191 GPa respectively. The Thomsen parameters are changing from UBSR to LBSR having an average value of − 0.0027 to − 0.0013, − 0.00026 to − 0.00029 and − 0.004 to − 0.002 respectively. The maximum value of epsilon is 0.022 showing strong zone of anisotropy for the gas-hydrate bearing zone and the minimum value is − 0.053 showing a weak anisotropy

Fig. 11 The computed elastic parameters such as shear modulus, young are modulus and bulk modulus for NGHP-01-09 using synthetic shear wave data with BSR depth 2225 m. The lower values of elastic parameters are denoted by L at the depth intervals where fractures are observed from FMI log data to indicate presence of stress induced anisotropy
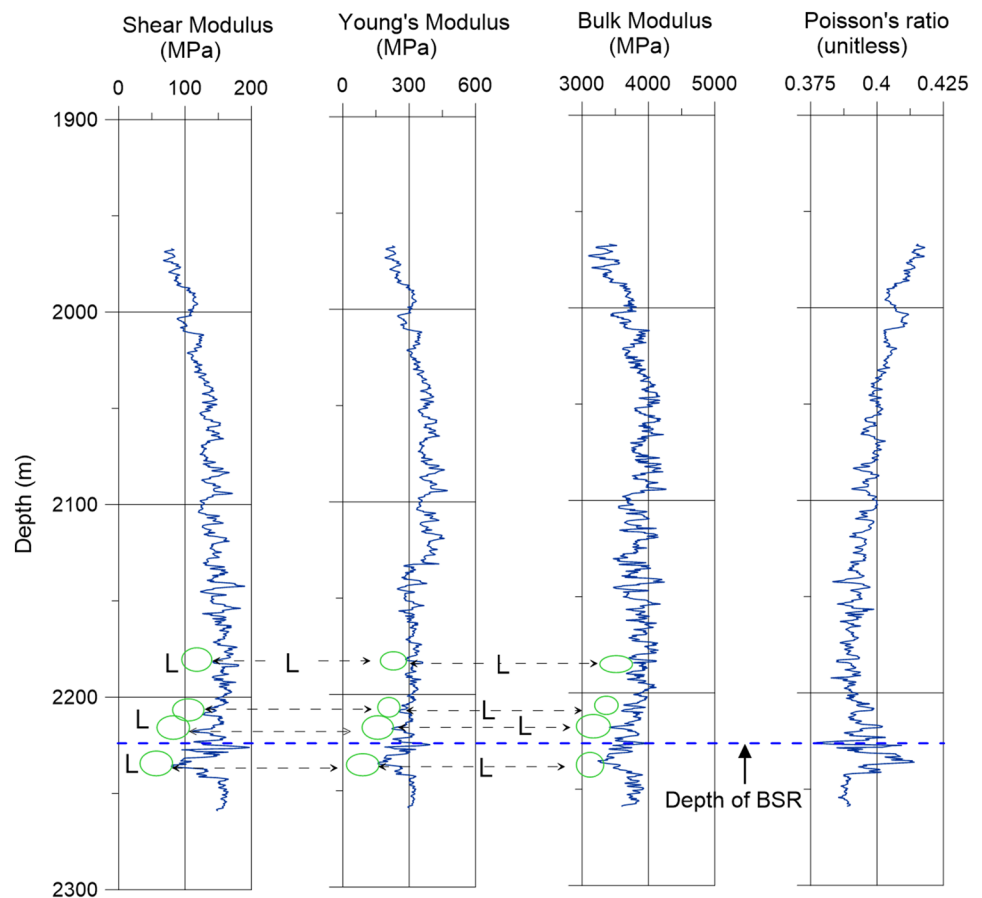
zone. The maximum value of epsilon in the gas hydrate stability zone (GHSZ) is 0.07 and the maximum value in the free gas zone is 0.19 showing a considerable amount of anisotropy in the gas hydrate-bearing zone and is strong in the underlying the free gas zone. Similarly, the maximum value of gamma in GHSZ is 0.01 and 0.5 in free gas zone showing anisotropy in free gas zone is stronger than GHSZ. The fracture density calculated from Thomsen's parameters showing higher values ranging from 0.039 to 0.076 are the strong anisotropy zones (Table 4). The fracture density values are varying from − 0.0731 to 0.0761 having an average value of − 0.0055 in the depth interval of 1493.11 m to 1690.32 m. The natural fractures have been observed using FMI log at same depth of higher fracture density having azimuth/orientation ranging from N166.15° to N360° in the depth interval of 1493.11 to 1690.32 m for the well NGHP-01-19.The natural dips for the well NGHP-01-19, NGHP-01-09 and NGHP-01-08 are 16.3°, 21.0° and 17.1° respectively. Further, the orientations of strong anisotropy are N320.4°, N344.6°, and N198.6° and the orientations of weak anisotropy are N351.5°, N345.7°, and N136.6°. The values of the elastic parameters such as shear modulus, young's modulus and bulk modulus increase from 291.60 to 580.38 MPa, 268.33 to 565.38 MPa and

3634.57 to 3780.55 MPa from the UBSR to LBSR and the value of Poisson's ratio slightly decreases from 0.486 to 0.474 in the depth range of 1493.11 to 1690.32 m for the well NGHP-01-19. It is observed that the values of elastic parameters decrease while fracture density increases and vice-versa which are shown in Table 4.

For other two wells, the values of elastic parameters increase from 119.53 to 143.97 MPa, 354.36to 423.97 MPa and 3392.88 to 3680.26 MPa respectively in the depth interval 1935.02 to 2258.87 m from UBSR to LBSR and whereas, the value of Poisson's ratio changes from 0.483 to 0.480 for well NGHP-01-09 for the corresponding depth of intervals. The values of elastic modulus are varying from 125.69 to 164.05 MPa, 372.82 to 485.43 MPa and 3760.69 to 4021.62 MPa respectively in depth interval of 1700.08 to 2031.86 m with the corresponding value of Poisson's ratio is varying from 0.484 to 0.480 for well NGHP-01-08.

Discussion

High velocities (~ 1.64 km/s) are achieved with high gas hydrate concentrations (~ 10–12%) just above the BSR depth (~ 208mbsf) and lower velocity (1.44 km/s) is found

Fig. 12 The computed elastic parameters such as shear modulus, young' s modulus and bulk modulus for NGHP-01-08 using synthetic shear wave data with BSR depth 1957 m. The lower values of elastic parameters are denoted by L at the depth intervals where fractures are observed from FMI log data to indicate presence of stress induced anisotropy in the well
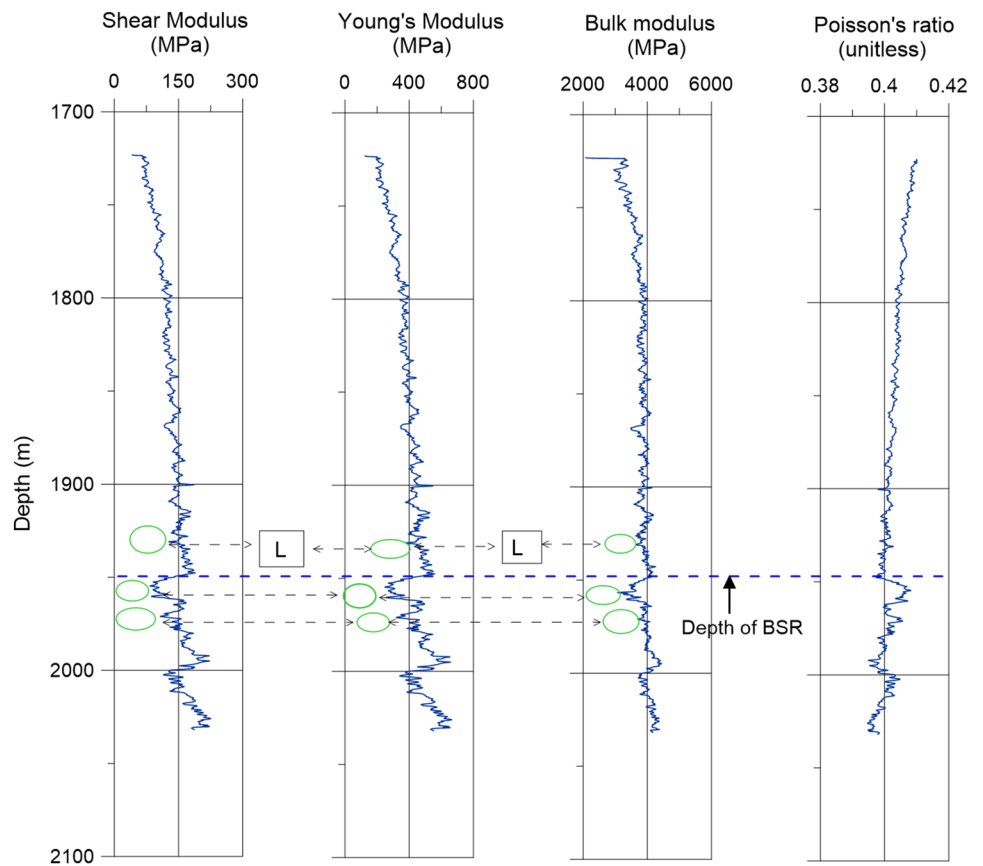
at depth ~ 1650 m just below it because of the presence of free gas in the well NGHP-01-19. The clay/silt layer which is also present in the un-compacted sediments may also be responsible for intrinsic causes of generating the anisotropy. One could assume a VTI medium for analyses of the anisotropy parameters but because of small thickness of shale layer we did not consider VTI medium in our study. Presence of natural fracture, pore filling gas hydrates and as well as change of mechanical behavior play a major role in generating stress-induced anisotropy and therefore, the analysis of anisotropy was done by assuming an HTI medium in the study area. The anisotropy is dominantly stress-induced than shale based in the gas-hydrate bearing sediments in the wells NGHP-01-19. These natural fractures are filled with solid gas hydrate or free gas, free water or pore filling solid matrix. The value of normal fracture weakness (δ_N) i.e. inverse of stiffness coefficient is high (high fracture density) showing the degree of anisotropy to be high or strong (Sill et al. 2012) shown in Fig. 10.

Crossplot between elastic parameters and fracture density

We have tried to classify the degree of anisotropy in well NGHP-01-19 based on the cross plot between the fracture density and elastic parameters. From Fig. 13, it is observed that the low value of elastic parameters and high value of fracture density (> 0.03) demarcate for strong anisotropy (SA) zone marked by the red box; intermediate values with fracture density (range $- 0.02$ to 0.03) represent for medium anisotropy (MA) zone marked by the yellow box and high elastic values and low fracture density ($< - 0.02$) indicate weak anisotropy (WA) zone marked by the green box. Thus, the fracture density is inversely proportional to the rock elastic parameters. The anisotropy is more sensitive to shear modulus and young's modulus than bulk modulus because anisotropy changes with size and shapes rather than with its volume. Therefore, we obtain sharp changes in shear and young's modulus from weak to high anisotropy zone above and below the BSR.

Table 4 Correlation of fracture density with natural fracture orientations and elastic parameters (Shear, Young's and Bulk moduli) for the depth interval of strong anisotropy zone at well NGHP-01-19

| Serial no.	Depth range (m)	Dip (°)	Azimuth (°)	Fracture density	Poisson's ratio	Shear modulus (MPa)	Young's modulus (MPa)	Bulk modulus (MPa)
1	1554.071–1554.985	14.2	360	0.049	0.487	88.48	263.21	3522.04
2	1558.033–1558.948	19.21	278.18	0.055	0.486	94.33	280.49	3545.31
3	1590.19–1591.104	10.82	360	0.039	0.490	61.35	182.99	3513.31
4	1601.01–1601.924	12.15	360	0.049	0.485	109.70	325.95	3843.09
5	1623.108–1623.87	26.25	218.22	0.060	0.479	151.39	447.81	3562.32
6	1626.004–1626.918	22.28	271.73	0.054	0.483	124.52	369.63	3932.81
7	1633.014–1633.928	14.07	360	0.065	0.479	165.45	489.90	4248.53
8	1643.072–1643.987	21.29	284.88	0.041	0.471	206.55	607.69	3522.13
9	1652.094–1652.978	18.69	192.5	0.044	0.479	157.06	464.68	3786.64
10	1668.066–1668.98	12.97	285.22	0.074	0.465	262.86	770.18	3721.83
11	1675.076–1675.991	10.80	263.05	0.076	0.475	189.44	558.42	3750.45
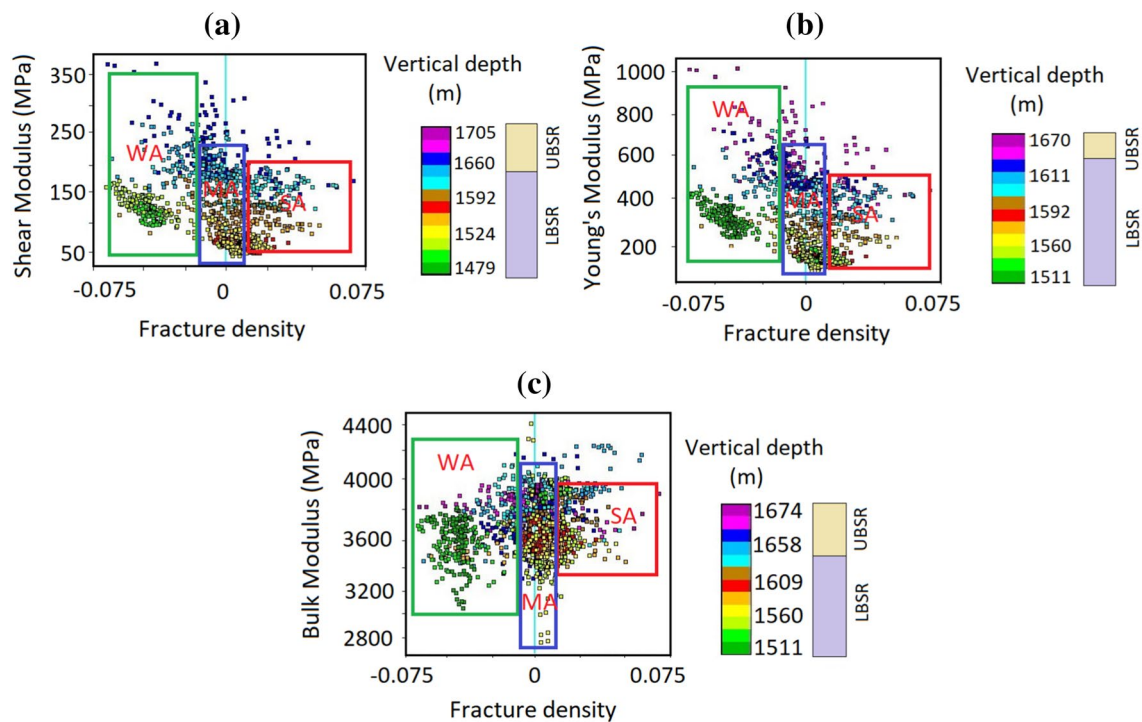
Fig. 13 Cross plot between fracture density between elastic parameters **a** fracture density vs. shear modulus, **b** fracture density vs. young's modulus and **c** fracture density vs. bulk modulus. Three type anisotropy zones classified which strong anisotropy (SA) mark by red colour, followed by medium anisotropy (MA) by yellow colour and weak anisotropy (WA) by green colour with corresponding depth range for well NGHP-01-19

Effect of gas hydrate and the relation of Thomsen's parameters

The cross-plots between fracture density with epsilon and gamma giving high correlations suggests that these values are directly proportional to each other while fracture density with epsilon is more correlated ($R^2 \sim 0.99$) than gamma suggesting that P-wave anisotropy is more effective than S-wave anisotropy. In this area the P-wave velocity is more affected by the anisotropy properties as shown in Fig. 14.

The anisotropy parameters are substantially influenced by the presence of fracture in gas hydrate sediments. The large negative values of epsilon and delta with positive
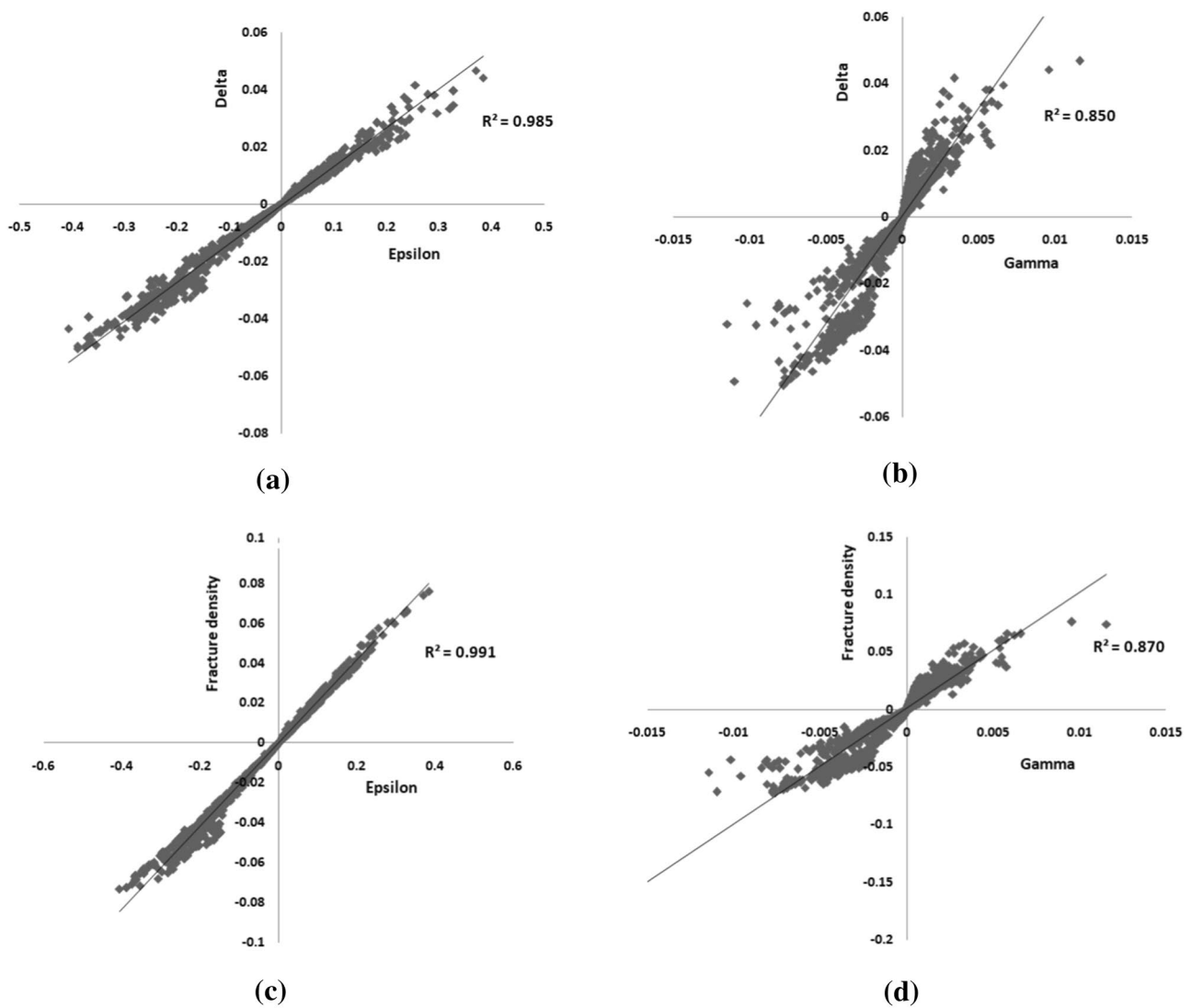
Fig. 14 Cross plot correlation between fracture density and Thomson's parameters **a** delta vs epsilon, **b** delta vs gamma, **c** fracture density vs epsilon and **d** fracture density vs gamma. These correlations show P-wave anisotropy is slightly higher than S-wave anisotropy while fracture density is collinear with Thomson's parameters such as epsilon and gamma

gamma represents either dry solid gas hydrate or free gas filled in the crack or fracture of the sediments, whereas small negative values represent wet filled cracks. The positive correlation between epsilon and gamma may be caused by an organic mixture of silt/clay-bearing sediments along with micro-fracture of the layer.

Velocity modeling using Thomsen's parameter

P-wave anisotropy is slightly more sensitive to S-wave anisotropy because of P-wave velocity in liquid phase as well as solid phase have greater sensitivity than S-wave velocity (shear modulus in fluid is zero) as reported in Wang 2002. Generally, P-wave anisotropy is slightly higher than S-wave anisotropy (Tsvankin 1996 and Peacher et al. 2003).

The simplified direction-dependent P-wave, SV- and SH-wave velocity for the angle of fracture angle 0°, 16.3° and 90° at well NGHP-01-19 as was given by Thomson's (1986) as follows;

$$V_P(\theta) \approx V_{P0}(1 + \delta\sin^2\theta\cos^2\theta + \varepsilon\sin^4\theta) \qquad (27)$$

$$V_{SV}(\theta) \approx V_{S0}\left[1 + \left(\frac{V_{P0}}{V_{S0}}\right)^2 (\varepsilon - \delta)\sin^2\theta\cos^2\theta\right] \qquad (28)$$

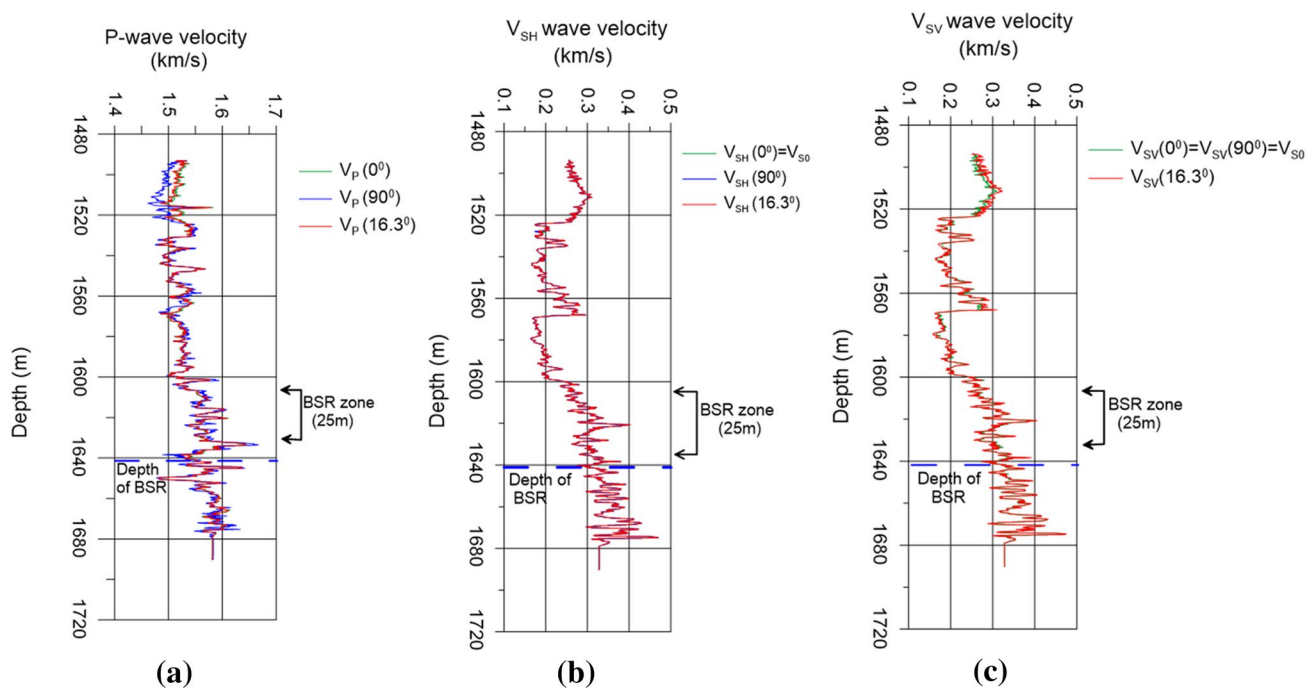$$V_{SH} \approx V_{S0}(1 + \gamma\sin^2\theta) \qquad (29)$$

where,

Fig. 15 Modeled **a** P-wave, **b** SH and **c** SV-wave using estimated stiffness coefficients and Thomsen's parameters for fracture angle minimum (0°), maximum (90°) and orientation of strong anisotropy (16.3°) relative to symmetry axis at NGHP-01-19

$$V_{P0} = \sqrt{\frac{C_{33}}{\rho}}; \quad V_{S0} = \sqrt{\frac{C_{44}}{\rho}}$$

To estimate the velocities at NGHP-01-19 sites, we considered three cases of different angle which are at minimum (0°), maximum (90°) and the third one, the average dip of fracture (16.3°) for strong anisotropy followed by using all the computed stiffness and Thomsen's parameters. Due to availability of velocity along the direction of 0°, 90°, and 16.3°, we have chosen 0°, 16.3° and 90° for velocity modeling in anisotropy medium. In the Fig. 15a, it is observed that Vp(90°) is more influenced and effected by anisotropic parameters than Vp(16.3°) in the gas hydrate and free gas sediments near BSR. The value of Vp(90°) has increased 1.5% to 2.5% whereas, the value of Vp(16.3°) has enhanced little bit ranging from 0.2 to 0.35% relative to P-wave velocity. Direction dependent shear wave velocities such as V_{SV} (0°), V_{SV} (16.3°), V_{SV} (90°) and V_{SH} (0°), V_{SH} (16.3°), V_{SH} (90°) are less effective in the presence of the anisotropy parameters as observed in the Fig. 15b, c.

Conclusions

We estimated the Thomsen's parameters accomplished with five stiffness coefficients assuming an HTI medium using upper and lower mode shear wave data at NGHP-01 site in the offshore Mahanadi basin. The anisotropic parameters along with fracture density and coefficient of anisotropy reveal a strong anisotropy zone near above and below the BSR because of the presence of gas hydrates and free gas or pore filling fracture. The maximum fracture density reaches 0.07 while the coefficient of anisotropy is 0.32 indicating a strong anisotropy zone. The strong anisotropy zones are also correlated with the natural fractures which are observed from FMI data in the study area. The elastic parameters of un-compacted marine sediments are also affected by stress-induced anisotropy reducing lower values of elastic modulus in the gas hydrate and free gas zones. The cross-plot analysis reveals that the strong, medium and weak anisotropy are classified with elastic parameters. The P-wave velocity has been modified by the inclusion of gamma and delta for accurate assessment of gas hydrates and has increased its value up to 2.8% from log velocity for 90° angle of fracture relative to symmetry axis. The stress induced an isotropy in gas hydrate bearing marine sediments is mostly caused by natural fractures/joints, change of mechanical behavior and pore-filling in clay/silt marine sediments in the study area.

References

Bastia R, Nayak P (2006) Tectonostratigraphy and depositional patterns in Krishna offshore basin, Bay of Bengal. Lead Edge 25:839–845

Bastia R et al (2010) Structural and tectonic interpretation of geophysical data along the eastern continental margin of India with a special reference to deep water petroliferous basins. J Asian Earth Sci 39:608–619

Bastia R, Radhakrishna M, Srinivas T, Nayak S, Nathanial DM, Biswal T, Bidgoli MN, Jing L (2014) Anisotropy of strength and deformability of fractured rocks. J Rock Mech Geotech Eng 6:156–164

Bidgoli MN, Jing L (2014) Anisotropy of strength and deformability of fractured rocks. J Rock Mech and Geotech Eng 2014:6(2)

Biksham G, Subramanian V (1988) Sediment transport of the Godavari river basin and its controlling factors. J Hydrol 101:275–290

Chatterjee R, Singha DK (2018) Stress orientation from image log and estimation of shear wave velocity using multiple regression model: a case study from Krishna-Godavari basin, India. J Indian Geophys Union 22:128–137

Coffin R, Pohlman J, Gardner J, Downer R, Wood W, Hamdan L, Walker S, Plummer S, Gettrust J, Diaz J (2007) Methane hydrate exploration on the mid Chilean coast: a geochemical and geophysical survey. J Petrol Sci Eng 56:32–41

Collett TS, Riedel M, Cochran J, Boswell R, Presley J, Kumar P, Sathe A, Sethi A, Lall M, Sibal V (2008) The NGHP expedition 01 scientists, national gas hydrate program expedition 01 initial reports. Directorate General of Hydrocarbons, New Delhi

Cook AE, Goldberg D, Kleinberg RL (2008) Fracture-controlled gas hydrate systems in the northern Gulf of Mexico. Mar Pet Geol 25:932–941. https://doi.org/10.1016/j.marpetgeo.2008.01.013

Cook A, Anderson B, Malinverno A, Mrozewski S, Goldberg D (2010) Electrical anisotropy due to gas hydrate-filled fractures. Geophysics 75(6):173–185. https://doi.org/10.1190/1.3506530

Das B, Chatterjee R (2018) Mapping of pore pressure, in-situ stress and brittleness in Unconventional Shale Reservoir of Krishna-Godavari Basin. J Nat Gas Sci Eng 50:74–89

Das S, Mohan S, Waraich RS (2010) Success, challenges and pitfalls in deep offshore Mahanadi Basin, East Coast of India. Oct 31–Nov 3, New Delhi, India, Paper Id: 20100583, Petrotech

Ekstrom MP, Dahan CA, Chen MY, Lloyd PM, Rossi DJ (1987) Formation imaging with microelectrical scanning arrays. Log Anal 28:294–306

Esmersoy C, Boyd A, Kane M, Denoo S (1995) Fracture and stress evaluation using dipole shear anisotropy logs. In: SPWLA 36th annual logging symposium, Paris, June 28–29

Fang X, Fehler M, Zhu Z, Chen T, Brown S, Cheng A, Toksoz MN (2013) An approach for predicting stress-induced anisotropy around a borehole. Geophysics 78:143–150. https://doi.org/10.1190/geo2012-0145.1

Fuloria RC (1993) Geology and hydrocarbon prospects of Mahanadi Basin, India. In: Proceedings of the 2nd seminar on "Petroliferous Basin in India", vol 3, Indian Petroleum, Publication, Dehra Dun, pp 355–369

Fuloria RC, Pandey RN, Bhavali BR, Mishra JK (1992) Stratigraphy, structure and tectonics of Mahanadi offshore basin. J Geol Surv India 29:255–265

Ghosh R, Kalachand S, Ojha M (2010) Effective medium modeling of gas hydrate filled fractures using the sonic log in the Krishna-Godavari basin, offshore eastern India. J Geophys Res 115:B06101. https://doi.org/10.1029/2009JB006711

Gupta IN (1973) Preliminary variations in *S*-wave velocity anisotropy before earthquakes in Nevada. Science 182:1123–1136

Hudson JA (1980) Overall properties of a cracked solid. Math Proc Cambridge Philos Soc 88:371–384. https://doi.org/10.1017/S0305004100057674

Jagannathan CR, Ratnam C, Baishya NC, Dasgupta U (1983) Geology of offshore Mahanadi Basin. Petroleum Asia J 6:101–104

Jaeger JC, Cook NWG (1979) Fundamentals of rock mechanics, 3rd edn. Chapman & Hall, New York

Kumar D, Sen MK, Bangs NL, Wang C, Pecher I (2006) Seismic anisotropy at Hydrate Ridge. Geophys Res Lett 33:L01306. https://doi.org/10.1029/2005GL023945

Kumar P, Collett TS, Boswell R, Cochran JR, Lall M, Mazumdar A, Ramana MV, Ramprasad T, Riedel M, Sain K, Sathe AV, Vishwanath K, Yadav US (2014) Geologic implications of gas hydrates in the offshore of India: Krishna Godavari Basin, Mahanadi Basin, Andaman Sea, Kerala Konkan Basin. Marine Pet Geol 58:29–98

Lee MW, Collett TS (2012) Characteristics and interpretation of fracture-filled gas hydrate-an example from the Ulleung Basin, East Sea of Korea. J Marine Pet Geol 47:168–181

Liu E, Li X-Y, Queen JH (2000) Discrimination of pore fluids from P and converted shear-wave AVO analysis. In: Ikelle L, Gangi A (eds) Anisotropy 2000: fractures, converted waves and case studies. Proceedings of the ninth international workshop on seismic anisotropy, SEG, pp 203–221.

Mavko G, Chan C, Mukerji T (1995) Fluid substitution: estimating changes in Vp without knowing Vs. Geophysics 60:1750–1755

Mohammed YA, Zillur R (2001) A Mathematical Algorithm for Modeling Geomechanical Rock Properties of the Khuffand Pre-Khuff Reservoirs in Ghawar Field. SPE Middle East Oil Show, Bahrain, March 17–20, Paper id: SPE68194

Musgrave MJP (1970) Crystal acoustics: Holden day.

Ostadhassan M, Zeng Z, Jabbari H (2012) Anisotropy analysis in shale using advance sonic data-Bakken case study. In: AAPG annual convention and exhibition, Long Beach, California

Peacher IA, Holbrook WS, Sen MK, Lizarralde D, Wood WT, Hutchinson DR, Dillon WP, Hoskins H, Stephen RA (2003) Seismic anisotropy in gas hydrate and gas bearing sediments on the Blake Ridge from a walk away vertical seismic profile. Geophys Res Lett 30:1733

Phillips SC, Flemings PB, Holland ME, Schultheiss PJ, Waite WF, Jang J, Petrou EG, Hammon H (2020) High concentration methane hydrate in a silt reservoir from the deep-water Gulf of Mexico. AAPG Bull. https://doi.org/10.1306/01062018280

Potter CC, Foltinek DS (1997) Formation elastic parameters by deriving S-wave velocity logs, CREWES report, 9, February 10–23

Prioul R, Donald A, Koespsell R, El Marzouki Z, Bratton T (2007) Forward modeling of fracture-induced sonic anisotropy using a combination of borehole image and sonic logs. Geophysics 72:135–147. https://doi.org/10.1190/1.2734546

Rai N, Singha DK, Shukla PK, Sain K (2020) Delineation of discontinuity using multi-channel seismic attributes: an implication for identifying fractures in gas hydrate sediments in offshore Mahanadi basin. Result Geophys Sci 1–4:100007

Rajabi M, Sherkati S, Bohloli B, Tingray M (2010) Subsurface fracture analysis and determination of in situ stress direction using FMI logs: an examples from the Santonian Carbonates (IIam fracture) in the Abadan Plain. Iran Tectophys 492:192–200

Ramana MV, Subrahmanyam V, Chaubey AK, Ramprasad T, Sarma KVLNS, Sastri VV, Venkatachala BS, Narayanan V (1981) The evolution of the east coast of India. Palaeogeogr Palaeoclimatol Palaeoecol 36:23–54

Rüger A (1998a) Variation of P-wave reflectivity with offset and azimuth in anisotropic media. Geophysics 63:935–947. https://doi.org/10.1190/1.1444405

Rüger A (1998b) Reflection coefficients and azimuthal AVO analysis in anisotropic media. Geophysical monograph series no. 10, Society of Exploration Geophysicists.

Ruger A (2002) Reflection coefficients and azimuthal AVO analysis in anisotropic media, Geophysical monograph series, Number 10, scociety of exploration geophysicists

Sain K, Gupta HK (2008) Gas hydrates: Indian scenario. J Geol Soc 72:299–311

Sain K, Gupta HK (2012) Gas hydrates in India: potential and development. Gondwana Res 22:645–657

Sain K, Rajesh V, Satyavani N, Subbarao KV, Subrahmanyam C (2011) Gas-hydrate stability thickness map along the Indian continental margin. Mar Pet Geol 28:1779–1786

Sain K, Ojha M, Satyavani N, Ramadass GA, Ramprasad T, Das SK, Gupta HK (2012) Gas hydrates in KG and Mahanadi basins: new data. J Geol Soc India 79:553–556

Sastri VV, Sinha RN, Singh G, Murti KVS (1973) Stratigraphy and tectonics of sedimentary basins on the east coast of penninsular India. AAPG Bull 57:655–678

Sastri VV, Venkatachala BS, Narayanan V (1981) The evolution of the east coast of India. Palaeogeogr Palaeoclimatol Palaeoecol 36:23–54

Satyavani N, Sen MK, Sain K (2013) Azimuthal anisotropy from OBS observation in Mahanadi offshore. India Interpret 1(2):187–198

Sayers CM (1994) The elastic anisotropy of shales. J Geophys Res Solid Earth 99:767–774

Sayers CM (2002) Stress-dependent elastic anisotropy of sandstones. Geophys Prospect 50:85–95. https://doi.org/10.1046/j.1365-2478.2002.00289

Sayers CM (2005) Seismic anisotropy of shales. Geophysics 64:93–98

Sayers CM, Kachanov M (1995) Microcrack-induced elastic wave anisotropy of brittle rocks. J Geophys Res 100:4149–4156. https://doi.org/10.1029/94JB03134

Schoenberg M, Sayers CM (1995) Seismic anisotropy of fractured rock. Geophysics 60:204–211. https://doi.org/10.1190/1.1443748

Shankar U, Pandey AK (2019) Estimation of gas hydrate saturation using isotropic and anisotropic modeling in the Mahanadi basin. J Earth Syst Sci 128:163

Shankar U, Riedel M (2014) Assessment of gas hydrate saturation in marine sediments from resistivity and compressional-wave velocity log measurements in the Mahanadi Basin, India. Mar Pet Geol 58:265–277

Shankar U, Gupta DK, Bhowmick D, Sain K (2013) Gas hydrate and free-gas saturations using rock physics modelling at site NGHP-01-05 in the Krishna-Godavaribasin, eastern Indian margin. J Petrol Sci Eng 106:62–70

Shaw RK, Sen MK (2006) Use of AVOA data to estimate fluid in a vertically fractured reservoir. Geophysics 71(3):15–24. https://doi.org/10.1190/1.2194896

Sil S (2012) Fracture parameter estimation from well-log data. Geophysics 78(3):129–134

Sil S, Keys RG, Roy B, Foster DJ (2012) Methods for seismic fracture parameter estimation and gas filled fracture identification from vertical well log data. U. S. Patent application 20,120,250,459.

Sil S, Srivastava R, Sen MK (2010) Observations of shear wave splitting in the multicomponent node data from Atlantis field, Gulf of Mexico. Geophys Prospect 58:953–964

Singha DK, Shukla PK, Chatterjee R, Sain K (2019) Multi-channel 2D seismic constraints on pore pressure- and vertical stress- related gas hydrate in the deep offshore of the Mahanadi Basin. India. J Asian Earth Sci 180:103882

Tatham RH, McCormack MD, Neitzel EB, Winterstein DF (1991) Multicomponent seismology in petroleum exploration. Society of Exploration Geophysicists, Tulsa, Oklahoma, p 248

Thomsen L (1986) Weak elastic anisotropy. Geophysics 51:1954–1966. https://doi.org/10.1190/1.1442051

Thomsen L (1999) Converted-wave reflection seismology over inhomogeneous, anisotropic media. Geophysics 64:678–690. https://doi.org/10.1190/1.1444577

Tsvankin I (1996) P-wave signature and notation for transversely isotropic media. An overview. Geophysics 61:467–483

Twiss RJ, Moores EM (1992) Structural geology. W.H. Freeman & Company, New York, p 532

Wang Z (2002) Seismic anisotropy in sedimentary rocks. Part 2. Laboratory data. Geophysics 67:1423–1440. https://doi.org/10.1190/1.1512743

Winkler KW (1996) Azimuthal velocity variations caused by borehole-stress concentrations. J Geophys Res 101:8615–8621. https://doi.org/10.1029/96JB00093

Yan J (2002) Reservoir parameters from well log and core data: a case study from the North Sea. Pet Geosci 08:63–69

Zoback MD, Moods D, Mastin L, Anderson RN (1985) Wellbore breakout and in situ stress. J Geophys Res 90:5523–5530